Electronic Supplementary Material (ESI) for Journal of Materials Chemistry A.
This journal is © The Royal Society of Chemistry 2014

<Supporting Information>

Synergetic effect of Graphene on Cu_2O Nanowire arrays as highly efficient hydrogen evolution photocathode in water splitting

Amare Aregahegn Dubale[1], Wei-Nien Su[2,*] Andebet Gedamu Tamirat[1], Chun-Jern Pan[1], Belete Asefa Aragaw[1], Hong-Ming-Chen[1], Ching-Hsiang Chen[2] and Bing-Joe Hwang[1,3*]

[1]NanoElectrochemistry Laboratory, Department of Chemical Engineering, National Taiwan University of Science and Technology, Taipei 106, Taiwan.
[2]NanoElectrochemistry Laboratory, Graduate Institute of Applied Science and Technology, National Taiwan University of Science and Technology, Taipei 106, Taiwan.
[3]National Synchrotron Radiation Research Center, Hsinchu 30076, Taiwan.
*Corresponding authors: bjh@mail.ntust.edu.tw; wsu@mail.ntust.edu.tw

Table S1 Raman shift positions and Intensity ratio (I_D/I_G) of Graphite, GO and graphene

	D-band (Lorentzian fit)		**G-band (Lorentzian fit)**		I_D/I_G
Materials	**Position cm^{-1}**	**fwhm cm^{-1}**	**Position cm^{-1}**	**fwhm cm^{-1}**	
Graphite	1346	46	1575	27	1.31
GO	1351	174	1593	99	1.52
Graphene	1344	132	1576	52	0.403
G-1.0/Cu_2O/ Cu mesh	1355	130	1603	71	0.85

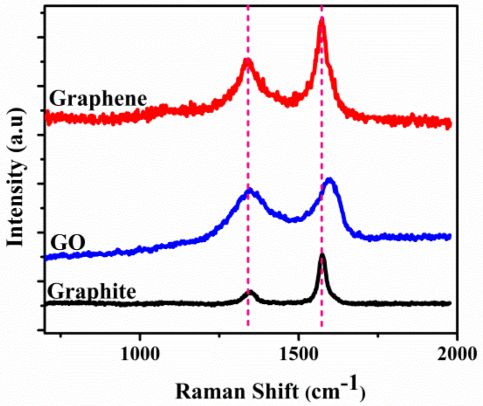

Fig. S1 Raman spectra of pristine graphite, graphene Oxide and graphene

The Raman spectrum on Fig. S1 shows, the D and G peaks which were found to be the most dominant in all the carbon materials. The G peak is due to the in plane stretching motion between sp^2 carbon atoms. The D band is recognized to be a disordered band originating in structural defects, edge effects and dangling sp^2 carbon bonds that break the symmetry. The D and G peak positions were determined by a Lorentzian fit after baseline subtraction.[1] For pristine graphite the, the D and G peak positions are centered at 1346 and 1575 cm^{-1} respectively, while for GO and graphene, these peaks are centered at 1351 and 1593 and at 1344 and 1576 cm^{-1} respectively. The D and G peak positions and I_D/I_G ratios of graphite, GO and graphene are summarized in Table S1.

As shown on Fig. S1 and Table S1, during oxidation followed by reduction of pristine graphite, the Raman peaks showed change in band shape and band position. During the conversion of graphite to GO, the D peak raises in intensity while the G peak widen and exhibit a shift to higher wavenumber (from 1575 to 1593 cm^{-1}) in GO than in graphite. The G peak in graphene is positioned nearly at the same wavenumber as that in graphite. The change in position of G- band to higher wavenumber during graphite amorphization indicates the presence of double bonds that resonate at higher wavenumber.[2] In graphene, the G band shifts back to the position of the G band in graphite (Fig. S1), which attribute to restoration of graphitic structure similar to what was observed from the sharpening of the G peak and the intensity decrease of the D peak in heat-treated graphite.[3, 4]

The integrated intensity ratio of the D and G-bands (I_D/I_G) of graphite, graphene oxide and graphene were found to be 0.403, 1.52 and 1.31 respectively. The higher intensity ratio of I_D/I_G of GO than that of pristine graphite confirms the oxidation of graphite. This is because, the D band increased during oxidation since oxygen functional groups were introduced into the graphitic chain. On the other hand, after the thermal reduction of GO to graphene, the I_D/I_G ratio was found to decrease. This indicates a considerable recovery of the conjugated graphitic framework upon de-functionalization of epoxide, hydroxyl and other oxygen containing functional groups during the thermal exfoliation process.[5, 6]

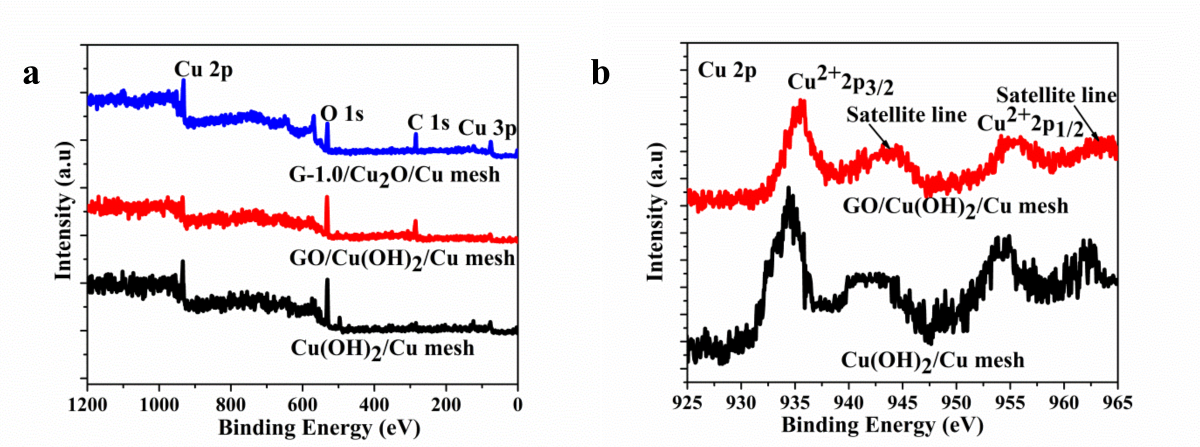

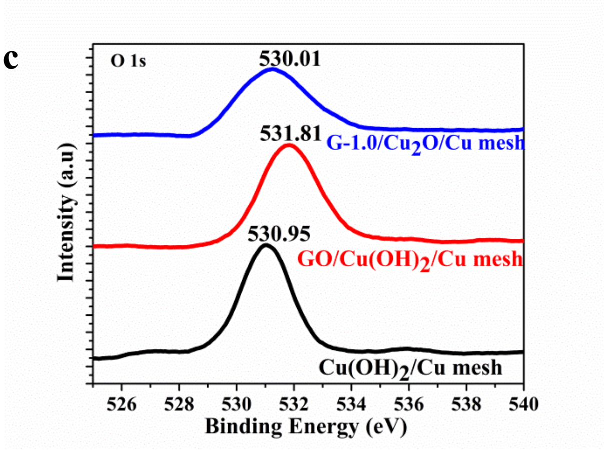

Fig. S2 XPS spectra of: (a) survey spectra of $Cu(OH)_2$/Cu mesh, GO/$Cu(OH)_2$/Cu mesh and G-1.0/Cu_2O/Cu mesh (b) Cu 2p core level of $Cu(OH)_2$/Cu mesh, Cu 2p core level of GO/$Cu(OH)_2$/Cu mesh (c) O 1s core level of $Cu(OH)_2$/Cu mesh, GO/$Cu(OH)_2$/Cu mesh and G-1.0/Cu_2O/Cu mesh.

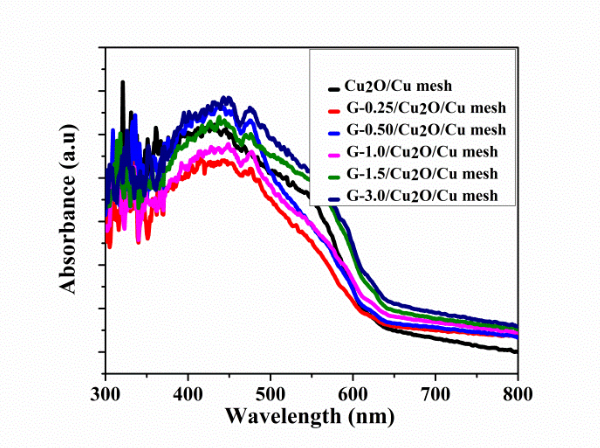

Fig. S3 UV-visible diffuse reflectance spectra (DRS) of the Cu_2O/Cu mesh and G-x/Cu_2O/Cu mesh.

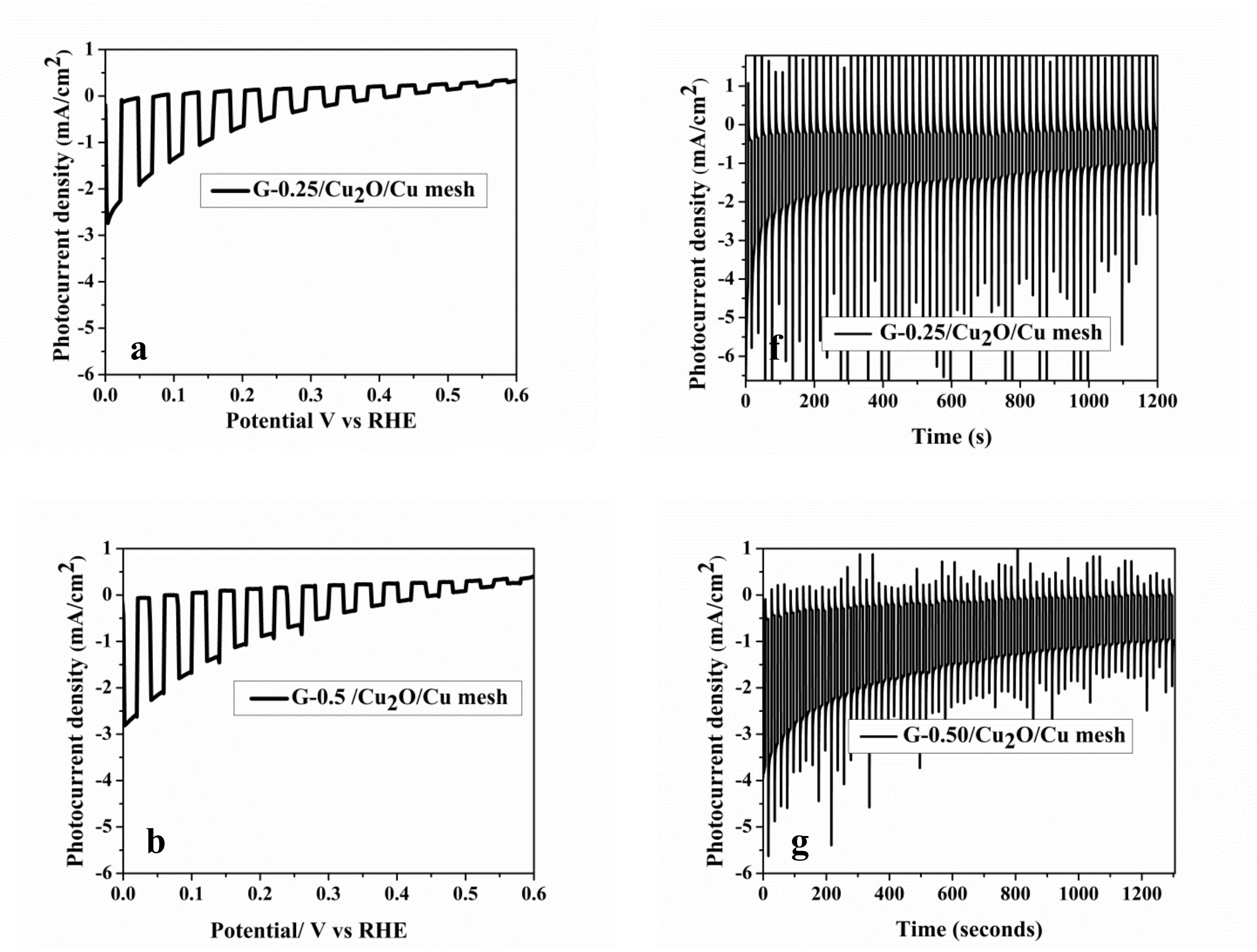

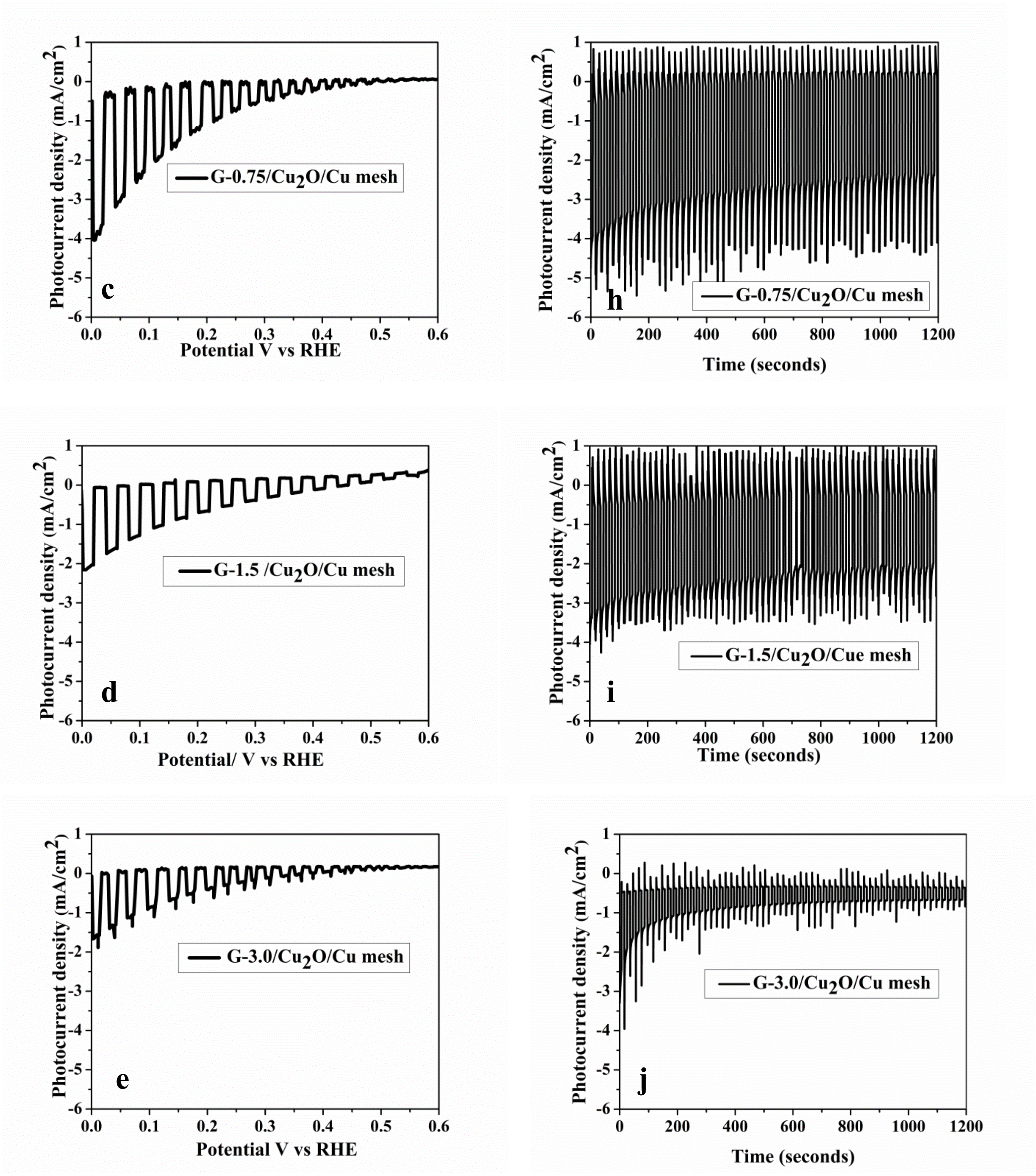

Fig. S4 PEC performances and stability measurement of (a, f) G-0.25/Cu_2O/Cu mesh; (b, g) G-0.5/Cu_2O/Cu mesh; (c, h) G-0.75/Cu_2O/Cu mesh; (d, i) G-1.5/Cu_2O/Cu mesh and (e, j) G-3.0/Cu_2O/Cu mesh

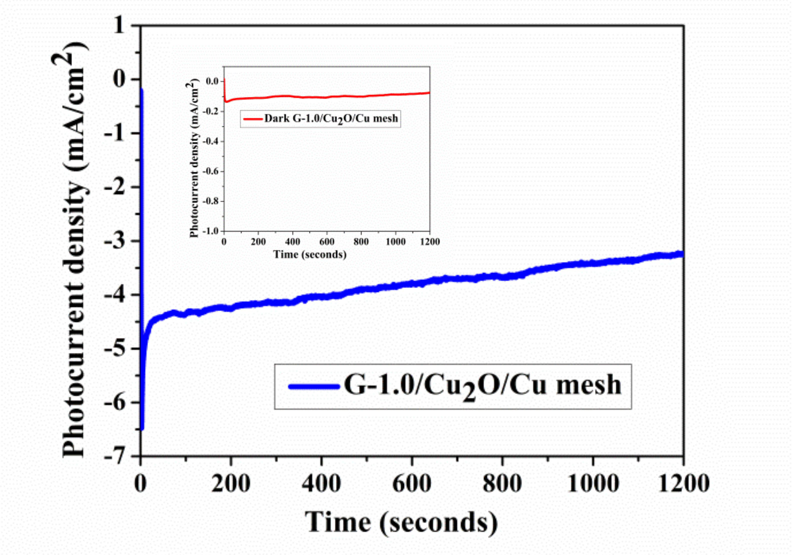

Fig. S5 Photocurrent density measurement of G-1.0/Cu$_2$O/Cu mesh at 0 V vs RHE under simulated one sun illumination during H_2 evolution experiment under continuous illumination and the inset plotted in Fig. S6 is for dark measurement

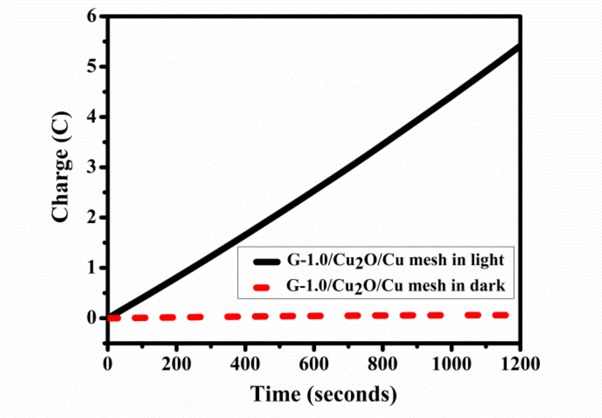

Fig. S6 Under dark (red dotted line) and visible light illumination (solid black line) electrolysis at an applied potential of 0 V vs RHE using G-1.0/Cu$_2$O/Cu mesh. The total charge was obtained from integration of the measured current over time using graphing software OriginPro 8.5

The chromatograms shown in Fig. S7 were for H_2 standard samples taken from 5% H_2/Ar (curve a to c) and our sample (curve d) obtained after PEC test for 20 minutes. Three point calibration (50, 100 and 150 μL of 5% H_2/Ar) was utilized to calibrate the GC before performing injection of our sample. Note that the chromatograms in Fig S7a (curve a to c), showed an increase in chromatographic peak area with increase in volume of standard H_2 sample. The peak areas of these curves were obtained by integration. Fig. S7b shows plot of peak area versus concentration of H_2 (calibration curve) accompanied by an acceptable correlation coefficient $r^2 = 0.9977$ is used to quantitate the hydrogen amount in the sample. After 20 minutes of photostability measurement, 50 μL of evolved gas was taken from head cup of the burret with air tight syringe and injected to GC. As clearly shown in curve d Fig S7a, the peak located at 1.2 minute exactly agree with the H_2 peak from the standards and is completely resolved from the rest of the peaks, confirming the presence of hydrogen. The strong peaks located at about 1.8 and 2.8 minutes corresponds to N_2 and O_2 respectively are consistent with literature report[7]. Nitrogen and oxygen take part 78 and 21% volume of dry air respectively; their presence cannot be neglected in separations detected with a PDHID[7]. Thus, the originated O_2 peak is probably due to gas leakage from air or reaction in closed system and N_2 from the purging N_2 gas and probably from air. The detection of H_2 in our sample is clearly showed by the enlargement of the peak (Fig. S7c).

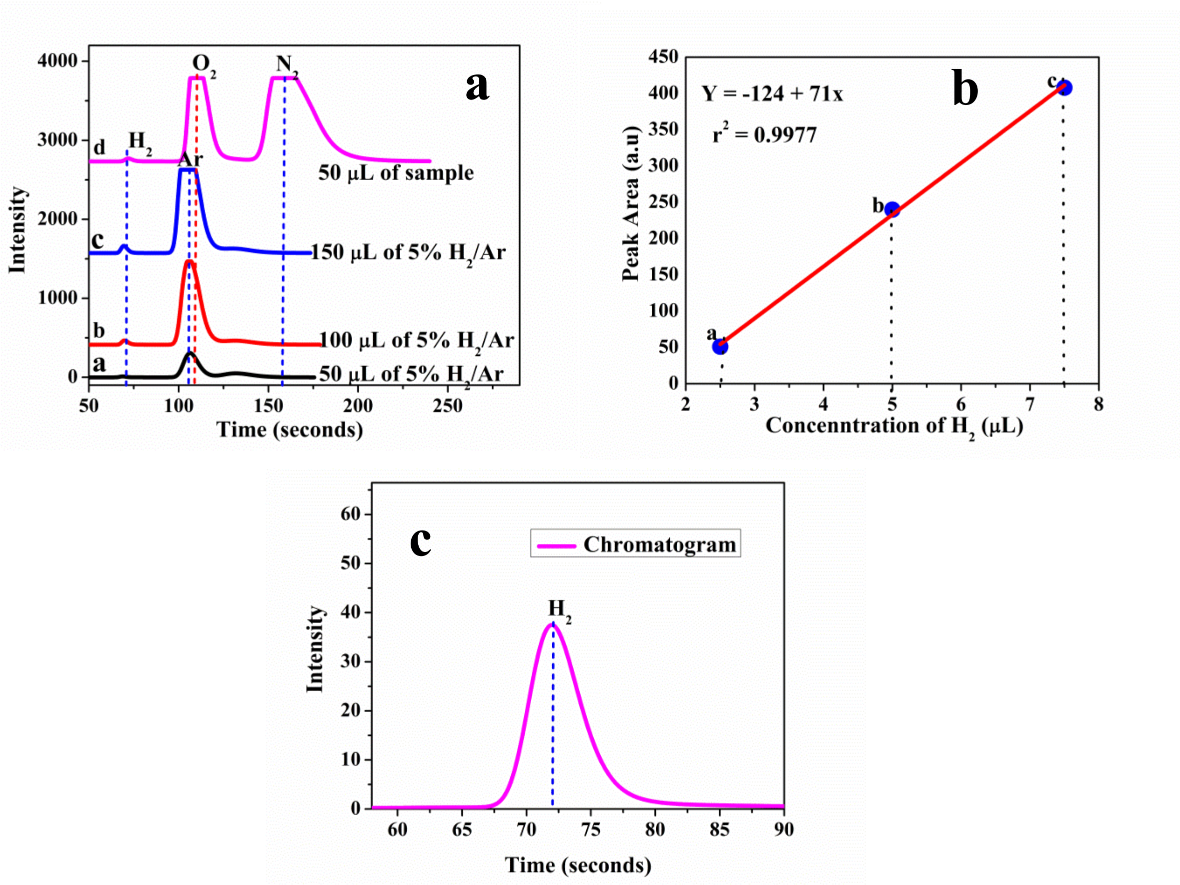

Fig. S7 (a) Chromatogram of standards (Curve a to c) and H_2 measurement for the photostability test (curve d) (b) Calibration curve of gas chromatography in this work (c) enlargement of curve d in Fig. S7a (H_2 region) from 60 to 90 seconds

The selected area in Fig. S8a clearly shows the fractured surface over the bare Cu_2O/Cu mesh where this problem is alleviated in presence of graphene in Fig. S8c. From Fig. S8c and 8d, the graphene modified photocathode (G-1.0/Cu_2O/Cu mesh) showed no clear difference in morphology before and after PEC, however, the bare Cu_2O/Cu mesh showed huge morphological change resulting bigger Cu nanoparticles over the surface, as seen in Fig 8b. This demonstrated that graphene play a role in suppressing photodegradation of Cu_2O nanowire arrays.

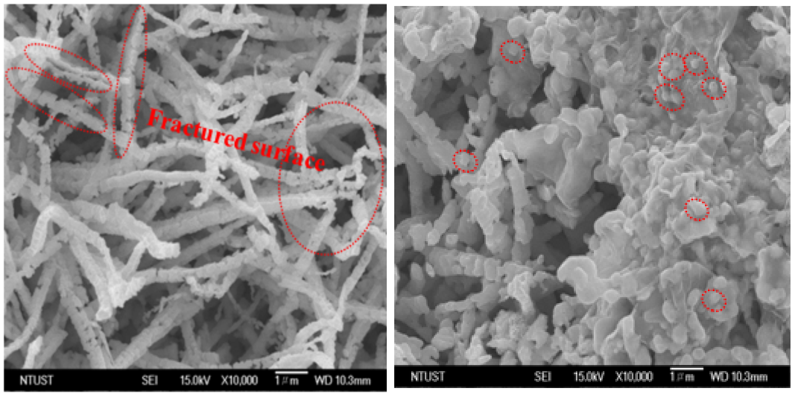

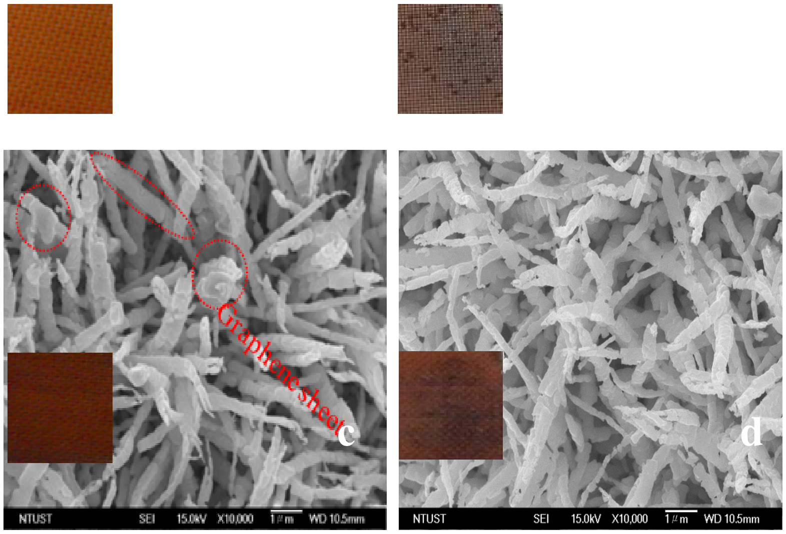

Fig. S8 FE SEM images and digital photograph (inset underneath) of Cu_2O/Cu mesh and G-1.0/ Cu_2O/Cu mesh before and after 20 minute photo-stability measurement under illumination of AM 1.5G (a) Cu_2O/Cu mesh before PEC (b) Cu_2O/Cu mesh after PEC (c) G-1.0/Cu_2O/Cu mesh before PEC and (d) G-1.0/Cu_2O/Cu mesh after PEC.

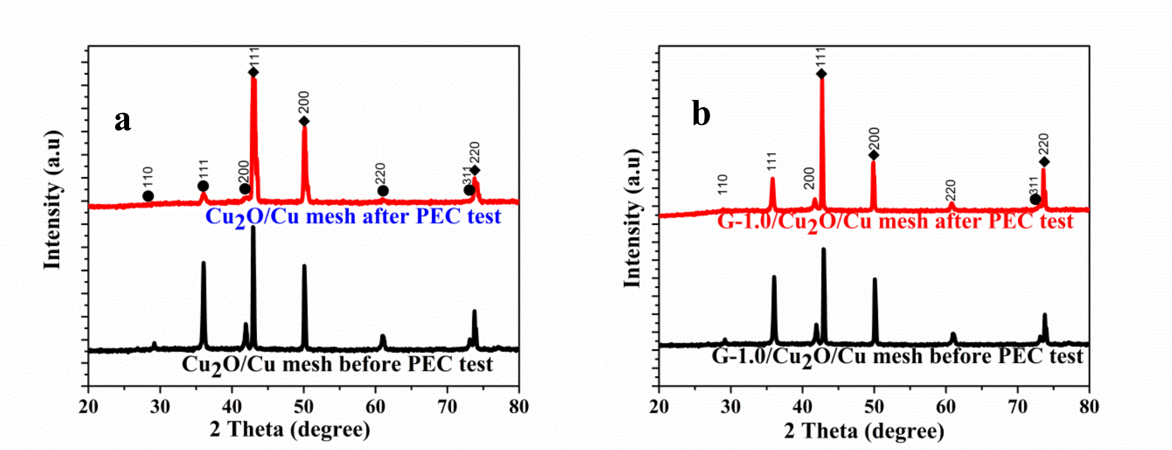

Fig. S9 XRD patterns of Cu_2O/Cu mesh (a) and G-1.0/Cu_2O/Cu mesh (b) before and after PEC test

It is well known that the PEC characterization in the three-electrode system give much more detailed information about the water reduction reaction. However, the application of three electrode system in determining a device measurement is quite limited. This is because; applying a bias with respect to a reference electrode excludes the second half reaction occurring on the counter electrode, which means that the PEC measurements with the applied bias versus the reference electrode only reveal an interface measurement instead of a device performance.[8] Thus, in this study we determined the applied bias photon -to- current efficiency (ABPE), which reveals the solar energy conversion efficiency with the electric energy deducted from the total efficiency, in the two electrode system by applying a bias between working and counter electrodes. The ABPE was estimated using the following expression:[8]

$$ABPE = \left[\frac{|J_{ph}|(mA/cm^2) \times (1.23 - |V_b|)(V)}{P_{total(mW/cm^2)}}\right]_{AM\,1.5G}$$

Where j_{ph} is the photocurrent density obtained under an applied bias Vb between the working and the counter electrodes in a two-electrode, 1.23 V is the standard water splitting reaction potential and P_{total} is the incident light intensity (which is 100 mW cm^{-2} in our case).

Fig. S10a shows the photocurrent density versus applied potential in the range from 0.05 V to –0.55 V (cathodic scan) with respect to Pt electrode in dark and under visible light irradiation at a scan rate of 10 mV. As can be seen in Fig. S10a, a dark scan from 0.05 to –0.55 V shows an almost negligible photocurrent density. Under light illumination an enhanced photocurrent density was observed over the entire potential which reached a maximum photocurrent density of –4.75 mA cm^{-1} at –0.55 V vs Pt electrode. The photocurrent density measurement at different potential vs Pt counter electrode shown in Fig. S10b is consistent with the results presented in Fig. S10a. The trend of the linear seep voltammetry curve measured in two electrode systems is also similar with LSV curve measured in three electrode systems. Fig. S10c shows a plot of ABPE against applied bias vs Pt electrode. As shown in Fig. S10c, the G-1.0/Cu_2O/Cu mesh showed maximum solar conversion efficiency (ABPE), 3.3%, at an applied bias of –0.55 V vs Pt counter electrode (Fig. S10a). The calculated ABPE value at different potential vs Pt counter electrode based on amperometric measurement performed for 20 minutes were also given in Fig. S10c and S10b respectively. As demonstrated in Fig. S10b and c, the magnitude of applied bias photon –to- current efficiency (ABPE) value is affected not only by the applied external biases but also by the generated photocurrent density.

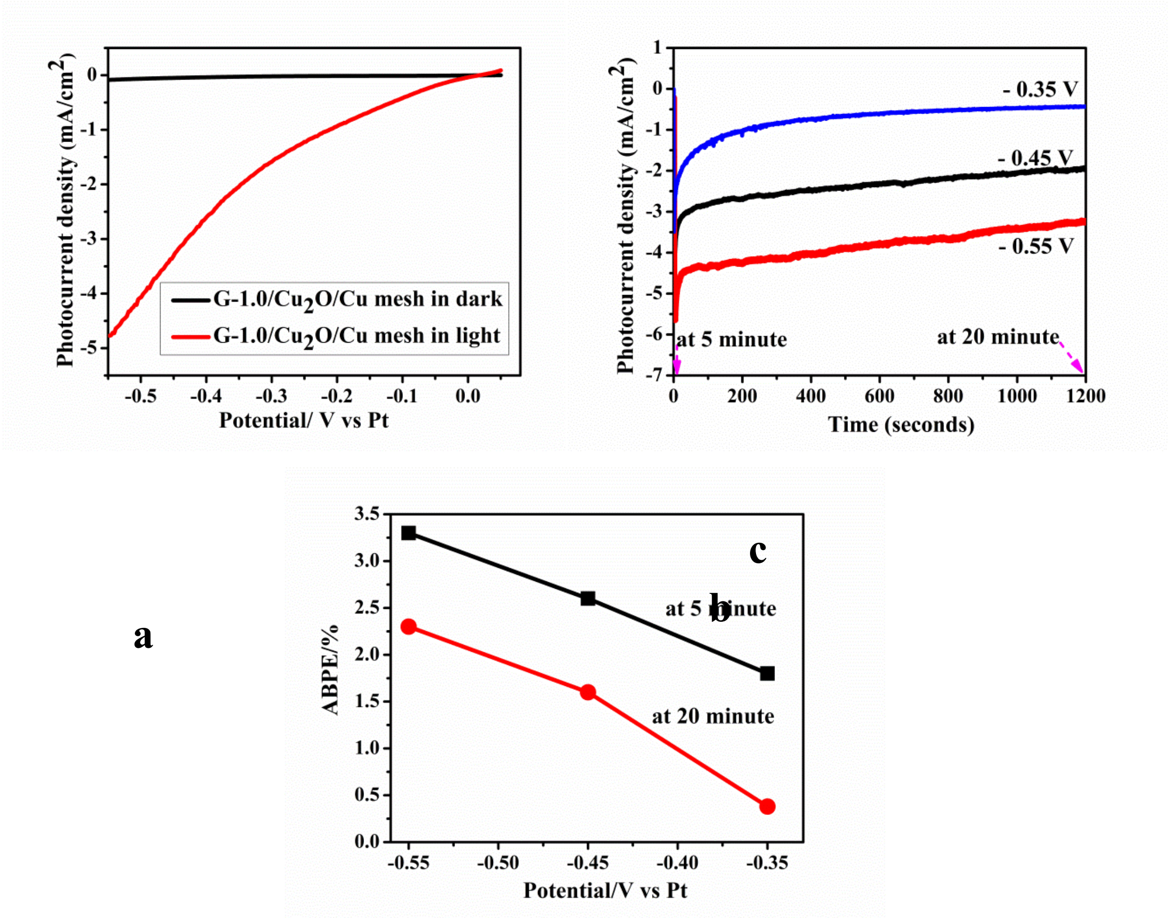

Fig. S10 Photoelectrochemical properties of G-1.0/Cu_2O/Cu mesh in two electrode system under simulated one sun illumination (100 mW cm^{-2}) (a) Linear sweep voltammetry (b) amperometric curves under different biases vs. Pt counter electrode (c) Applied bias photon-to-current efficiency (ABPE, %) vs Pt counter electrode

Reference:

1. A. J. Glover, M. Cai, K. R. Overdeep, D. E. Kranbuehl and H. C. Schniepp, *Macromolecules*, 2011, **44**, 9821-9829.
2. K. N. Kudin, B. Ozbas, H. C. Schniepp, R. K. Prud'homme, I. A. Aksay and R. Car, *Nano Letters*, 2007, **8**, 36-41.
3. K. Sato, R. Saito, Y. Oyama, J. Jiang, L. G. Cançado, M. A. Pimenta, A. Jorio, G. G. Samsonidze, G. Dresselhaus and M. S. Dresselhaus, *Chemical Physics Letters*, 2006, **427**, 117-121.
4. C.-C. Han, J.-T. Lee and H. Chang, *Chemistry of Materials*, 2001, **13**, 4180-4186.

5. V. Lee, L. Whittaker, C. Jaye, K. M. Baroudi, D. A. Fischer and S. Banerjee, *Chemistry of Materials*, 2009, **21**, 3905-3916.
6. A. Ambrosi, A. Bonanni, Z. Sofer, J. S. Cross and M. Pumera, *Chemistry – A European Journal*, 2011, **17**, 10763-10770.
7. M. T. Roberge, J. W. Finley, H. C. Lukaski and A. J. Borgerding, *Journal of Chromatography A*, Evaluation of the pulsed discharge helium ionization detector for the analysis of hydrogen and methane in breath, **1027**, 19-22.
8. Z. Chen, T. F. Jaramillo, T. G. Deutsch, A. Kleiman-Shwarsctein, A. J. Forman, N. Gaillard, R. Garland, K. Takanabe, C. Heske, M. Sunkara, E. W. McFarland, K. Domen, E. L. Miller, J. A. Turner and H. N. Dinh, *Journal of Materials Research*, 2010, **25**, 3-16.